The Cryosphere Discuss., doi:10.5194/tc-2016-202, 2016
Manuscript under review for journal The Cryosphere
Published: 26 September 2016

The Cryosphere Discussions
Open Access
EGU

Moderate mass loss of Kanchenjunga Glacier in the eastern Nepal Himalaya since 1975 revealed by Hexagon KH-9 and ALOS satellite imageries

Damodar Lamsal[1,a], Koji Fujita[1], Akiko Sakai[1]

[1]Graduate School of Environmental Studies, Nagoya University, Nagoya 464-8601, Japan
[a]now at: Asia Air Survey Co., Ltd., Tokyo 160-0023, Japan

Correspondence to: Koji Fujita (cozy@nagoya-u.jp)

Abstract. This study presents the geodetic mass balance of Kanchenjunga Glacier, a heavily debris-covered glacier, in the easternmost Nepal Himalaya between 1975 and 2010 using high-resolution (5-m) digital elevation models (DEMs) generated from Hexagon KH-9 and ALOS PRISM stereo-images. Glacier velocities are also calculated using a feature tracking method with two ALOS ortho-images taken in 2010. The difference between the two DEMs shows the rate of elevation change of the glacier, considerable surface lowering across the debris-covered area, and slight thickening in the accumulation area between 1975 and 2010. The velocity throughout the debris-covered area is slow, which stands in contrast with the faster velocity in the lower accumulation area. The rates of elevation change positively correlate with the elevation along the debris-free part, while they negatively correlate with elevation over the debris-covered part, which may result from the distribution of debris thickness. The rate of elevation change also positively correlates with the glacier velocity, whereas no correlation is found with slope and gradient of flow speed. Significant surface lowering is observed at supraglacial ponds, though the ponds should have short life spans. The geodetic mass balance of Kanchenjunga Glacier for the period of 1975–2010 (–0.14 ± 0.12 m w.e. a^{-1}) is considerably less negative than those estimated for Khumbu Glacier (–0.27 m w.e. a^{-1}) in the neighbouring Khumbu region. Disparities in the density of supraglacial ponds and the area contributions of accumulation and debris-covered areas may be principal causes of the difference in geodetic mass balance between the two glaciers.

1 Introduction

In recent decades, glaciers in the Himalayas, once one of the most glacierized mountainous areas in the world, were widely losing mass, though they exhibited a high degree of spatial heterogeneity (Fujita and Nuimura 2011; Bolch et al., 2012; Kääb et al., 2012; Gardelle et al., 2013). Studies on volumetric change in Himalayan glaciers have increased significantly in recent years, but there are still notable gaps spatially and temporally. For instance, glaciers in the Khumbu region of Nepal have been frequently studied (e.g. Nakawo et al., 1999; Bolch et al., 2011; Nuimura et al., 2011, 2012; Salerno et al., 2015). Khumbu Glacier is one of the most extensively studied glaciers in the Himalayas, while glaciers in the Kanchenjunga region (present study site) have been studied little and are thus poorly understood. Reasons for repeated investigations of the Khumbu region include easier access to glaciers, better logistic facilities, and the existence of Mt. Everest. While repeated investigations in a particular region or of a particular glacier help deepen our understanding of cryospheric processes, records from data-scarce regions are also important. Although Racoviteanu et al. (2015) investigated glacier surface area changes around the Kanchenjunga region between the 1960s and 2000s, no record of glacier mass changes has been reported from this

The Cryosphere Discuss., doi:10.5194/tc-2016-202, 2016
Manuscript under review for journal The Cryosphere
Published: 26 September 2016

region. In-situ monitoring programs often have shortcomings pertaining to their limited temporal and spatial coverage, whereas, despite their large spatial coverage, modern satellite observations are also limited to mostly after the year 2000. Declassified US spy satellite data (e.g., Corona KH-4 and Hexagon KH-9 stereo-images) are available for certain periods between the 1960s and the mid-1980s for many glacierized areas of the globe, and there are now several modern satellite datasets. Digital elevation models (DEMs) can be generated from both of these data sources. These DEMs of multi-decadal time-lapse allow us to investigate the long-term mass change of glaciers (Pieczonka et al., 2013; Ragettli et al., 2016).

Many glaciers in the Himalayas are characterized by the presence of supraglacial debris cover in their ablation areas (i.e., debris-covered glaciers) whose responses to climate change are more complicated than those of debris-free glaciers because of the insulation effect of the debris mantle (Scherler et al., 2011), the inhomogeneous distribution of debris thickness (Han et al., 2010; Zhang et al., 2012), and the presence of supraglacial ponds and ice cliffs (Sakai et al., 1998, 2000, 2002). Earlier studies have reported that variation in debris thickness resulted in different rates of ice melting through factors primarily responsible for forming ice cliffs and supraglacial ponds that significantly contributed to intense ice wastage (Sakai et al., 2000; Röhl, 2008; Han et al., 2010; Steiner et al., 2015; Miles et al., 2016). However, those observations were not performed at the spatial scale of an entire glacier but were limited to several ice cliffs and supraglacial ponds. This is because supraglacial ponds and ice cliffs, which are small-scale landform features on the glacier surface, require high-resolution (e.g., in-situ) observations; many ice cliffs and supraglacial ponds on large and dynamic debris-covered glaciers, however, are either physically inaccessible or too hazardous to conduct direct measurements. In addition, remote sensing-based global DEMs such as SRTM and ASTER GDEM2 are inadequate for representing these small features because of their coarse resolutions.

This study therefore aims to document the geodetic mass change of Kanchenjunga Glacier (27.70–27.88°N, 88.01–88.20°E), a large and heavily debris-covered glacier in a data-scarce region in the easternmost Nepal Himalaya (Fig. 1), over recent decades using historical and recent satellite images. This glacier has an extensive supraglacial debris mantle from the terminus to 19 km up-glacier, covering about 15 km^2 of the surface area and has six major tributaries (defined clockwise as T1 to T6). It is also aims for a better understanding of the effects of supraglacial ponds and other factors on ongoing changes in debris-covered glaciers under the recent climatic change.

2 Data and Methods

2.1 Data

Two sets of optical stereoscopic images (hereafter stereo-images), namely Hexagon KH-9 and Advanced Land Observing Satellite – Panchromatic Remote-sensing Instrument for Stereo Mapping (ALOS PRISM), are used in this study. Hexagon KH-9 has high spatial resolution (6 to 9 m) and wide geographic coverage (125 × 250 km). Mapping camera of Hexagon KH-9 took consecutive nadir imageries of the ground with about 70% overlap (Surazakov and Aizen, 2010; Pieczonka et al., 2013). Three KH-9 images taken in December 1975 (Table 1) are obtained from the Center for Earth Resources Observation and Science of the U.S. Geological Survey for DEM creation and mapping of glacier and supraglacial ponds.

Similarly, three pairs of ALOS PRISM images (spatial resolution of 2.5 m) along with rational polynomial coefficients (RPCs) data acquired from the Remote Sensing Technology Center of Japan are utilized (Table 1). These data were dated

The Cryosphere Discuss., doi:10.5194/tc-2016-202, 2016
Manuscript under review for journal The Cryosphere
Published: 26 September 2016

October 2008 for mapping supraglacial ponds of Khumbu Glacier, March 2010 for the initial image for velocity measurement of Kanchenjunga Glacier, and December 2010 for DEM generation, the final image for velocity measurements, and mapping glacier and supraglacial ponds of Kanchenjunga Glacier.

2.4 Glacier delineation and hypsometry

Boundaries of the glacier, debris-covered, and debris-free areas are manually delineated using Hexagon KH-9 (1975) and ALOS PRISM (2010) ortho-images . Uncertainty associated with the glacier surface delineation was estimated as an error of ±1 pixel along its perimeter (Fujita et al., 2009; Ojha et al., 2016). The glacier was divided into a set of elevation bands at intervals of 50 m to calculate area-weighted average of elevation and thus volume change. As the DEMs created in this study do not cover the entire glacier, ASTER GDEM2 (Tachikawa et al., 2011) is used to obtain the glacier hypsometry.

2.5 DEM generation from ALOS PRISM imagery

The ALOS PRISM images are processed with RPCs data, which contain information pertaining to interior orientations (specifics of the internal geometry of cameras or sensors such as focal length and principle point) and exterior orientations (e.g., position and tilt of camera/sensor) of the acquired images. With the use of stereo-images along with RPCs enables geometric modelling, thereby allowing the creation of digital terrain models (DTMs) and ortho-images, even without supplying ground control points (GCPs). With the aid of RPCs data and the Leica Photogrammetric Suite (LPS) Workstation, ALOS stereo-models and DTMs are generated. However, automatically extracted DTMs often contain many errors, especially in areas of highly irregular and abruptly changing topographies, such as high relief, shadows, and low contrast in the images, leading to an inaccurate terrain representation (Lamsal et al., 2011). Editing of mass points, which are sets of points with coordinate values defining the terrain surface, is therefore an important post-process for obtaining precise terrain representation. The major editing tasks performed include removing false spikes (mass points in the air) and depressions (mass points below the actual surface), and thus placing adequate and representative mass points exactly on the terrain surface. The LPS Terrain Editor was used to correct and minimize errors contained in the automatically generated DTMs. Finally, the extensively edited DTM was gridded into a DEM at a spatial resolution of 5-m (hereafter ALOS-DEM).

2.6DEM generation from Hexagon KH-9 imagery

Hexagon KH-9 images contain distortions due to development and duplication of the film as well as long-term storage. By correcting the distortions with the aid of reseau grids in the images, which allows accurate reconstruction of the image geometry, the images become suitable for DEM extraction (Surazakov and Aizen, 2010). Because RPCs are unavailable for Hexagon KH-9 images, GCPs are collected from the edited ALOS stereo-model. As both images used here have high spatial resolutions, terrain features such as boulders, trail intersections, and sharp notches on moraines are identifiable; thus, 21 GCPs are extracted from the off-the-glacier area, at which unchanged terrain is expected (Fig. 1). Five of the 21 GCPs are randomly selected and then used to validate the accuracy of affine transformation, which is 0.8 pixels (GCPv in Fig. 1). The same DTM editing is performed as that used for the ALOS DTM (Sect. 2.4). The generated DEM is resampled at the same spatial resolution of 5-m (hereafter Hex-DEM) as ALOS-DEM.

The Cryosphere Discuss., doi:10.5194/tc-2016-202, 2016
Manuscript under review for journal The Cryosphere
Published: 26 September 2016

2.7 Unmeasured upper accumulation area

The upper accumulation area of Kanchenjunga Glacier is extensively covered by snow, such that high brightness and poor contrast in both ALOS PRISM and Hexagon KH-9 images preclude the creation of DEMs for the entire glacier (37.5 km^2, 62% of the entire glacier). Therefore, continuous DEMs are available only for the lower 22.6 km^2 section (38% of the entire glacier), in which the debris-covered area is 15.0 km^2 and the debris-free area is 7.6 km^2. Owing to better local image contrast, patchy DEM creation is attainable at nine locations in the upper area (hereafter point sites, Fig. 2a). Two assumptions are used to estimate the rate of elevation change in the upper accumulation area where DEMs are unavailable (Table 2): 1) the average derived from nine point sites (+0.01 m a^{-1}, Figs. 2a and 3a) and 2) the average of the debris-free part above equilibrium-line altitude (ELA, 5800-5850 m a.s.l.; +0.11 m a^{-1}, Fig. 3a). Because the ELA of the glacier is unmeasured, it is assumed to be around 5800-5850 m, a rough estimate based on the geodetic elevation change, at which no change of glacier surface elevation is found for the studied period of 1975–2010 (hereafter gELA, Fig. 3a). Based on this assumption, the accumulation area ratio (gAAR) of Kanchenjunga Glacier is computed to be 0.54 (32.4 of 60.0 km^2).

2.8 Uncertainty estimates of the DEMs

Relative accuracy of the produced DEMs is evaluated as the elevation difference between two DEMs in the off-glacier area (1.7 km^2, Fig. 2a). The median, mean, and standard deviation of the elevation difference are 1.6, 1.1, and 5.5 m, respectively (Fig. 4), from which the uncertainty of the rate of elevation change is therefore estimated to be ±0.16 m a^{-1}. This relative accuracy is significantly smaller than those of previous studies performed in the Himalayas (Bolch et al., 2011; Nuimura et al., 2012; Gardelle et al., 2013). Accumulation areas of glaciers often consist of snow and ice, whereas ablation areas mostly contain ice, meaning that elevation change in an ablation area results in denser and thus more mass change than elevation change in an accumulation area. Although many studies have used a uniform ice density of about 900 kg m^{-3} for entire glaciers to convert surface elevation change into mass change (e.g., Bolch et al., 2011; Nuimura et al., 2012; Gardelle et al., 2013), a few recent studies have applied two different density assumptions, 900 kg m^{-3} for ablation areas and 600 kg m^{-3} for accumulation areas (e.g., Kääb et al., 2012; Pellicciotti et al., 2015). In this study, two ice density scenarios are considered: 1) 900 kg m^{-3} for the entire glacier area, and 2) 900 and 600 kg m^{-3} for the ablation and accumulation areas, respectively. The mean of these two scenarios is expected to provide the most plausible mass change estimate (Kääb et al., 2012). Taking into account the two density scenarios, the uncertainty in the mass change estimation is calculated to be ±0.12 m w.e. a^{-1}.

2.7 Glacier velocity

In order to investigate the effects of certain dynamics on changes in glaciers, the distribution of the surface velocity of Kanchenjunga Glacier is calculated using a feature tracking method, which is one of the most efficient methods used to derive glacier surface velocity or surface displacements (Heid and Kääb, 2012). Orthorectified pairs of ALOS PRISM images acquired in March and December of 2010 (9-month gap) are processed using the Co-Registration of Optically Sensed Images and Correlation (COSI-Corr) algorism, which is chosen because of its proven applications for deriving terrain displacement, including glacier velocity in mountainous regions (e.g., Leprince et al., 2007; Scherler et al., 2008). The COSI-Corr estimates the phase difference in the Fourier domain, allowing the computation of relative surface displacement between the initial image (reference image) and final image (search image). Stereo-images are firstly ortho-rectified, and then co-registered to

The Cryosphere Discuss., doi:10.5194/tc-2016-202, 2016
Manuscript under review for journal The Cryosphere
Published: 26 September 2016

ensure corresponding pixels in each image exactly overlap, which is required to initialize the matching process. Glacier velocity is computed using a correlation window of 64 × 64 pixels, corresponding to 160 × 160 m, a robustness iteration of 4, and a mask threshold for noise reduction of 0.9 (Leprince et al., 2007). To ensure the quality of the velocity map, poor matching in the surface displacements is removed by applying a correlation threshold of 0.6, which results in some voids in the shaded area (Fig. 2b). Details of the process and methodological background of COSI-Corr and its application to glacier-velocity computations are well documented by Leprince et al. (2007) and Scherler et al. (2008). The velocity distribution of Kanchenjunga Glacier is consistent with that of the produced DEMs because high brightness in the upper accumulation area severely hampers the identification and matching of surface features.

2.8 Supraglacial ponds

Supraglacial ponds and ice cliffs could enhance the melt of debris-covered ice by absorbing radiative heat as hot spots (Sakai et al., 2000, 2002; Steiner et al., 2015; Miles et al., 2016), such that their distribution density is important for better understanding the mechanisms of glacier degradation. Through the DTM editing used to create DEMs mentioned above, we simultaneously delineated supraglacial ponds on the glacier, which are rather easily identifiable with flat terrain features in stereo images, whereas it is difficult to distinguish ice cliff and debris-covered steep slopes on panchromatic images. In order to avoid misinterpretation of topography, we delineated ponds greater than 0.001 km^2 (12 × 12 pixels of ALOS image). For a comparison performed later, pond delineation was also conducted for Khumbu Glacier using the ALOS PRISM images taken in October 2008 (Table 1).

3 Results

3.1 Glacier area change

The surface area of Kanchenjunga Glacier was found to be 60.5 ± 1.6 km^2 in 1975 and 59.1 ± 0.5 km^2 in 2010, suggesting a 1.4 ± 0.1 km^2 (0.070 ± 0.006% a^{-1}) area loss for the studied 35 years. The average of areas in 1975 and 2010 (59.8 ± 1.1 km^2) is used for estimating the mass change of the glacier. Frontal retreat of the glacier is not noticeable, but two minor tributaries in the upper catchments, which were connected to the major tributaries in 1975, are retreated and disconnected by 2010 (T1 and T6, Fig. 1), leading to less significant area loss of the glacier. Considering the uncertainty in area delineation and the long time span of 35 years, the surface area loss of Kanchenjunga Glacier is negligible (2.3 ± 0.2%).

3.2 Changes in elevation and mass of the glacier

The distribution map of rate of elevation change is derived from Hex-DEM and ALOS-DEM; minus and plus signs denote glacier surface lowering (down-wasting) and thickening (Fig.2a), respectively. The most pronounced down-wasting is observed between 4700 and 5500 m a.s.l. (Fig. 3a). Overall, the glacier surface slightly lowered at the lowermost ablation area, remarkably lowered at the middle ablation area, and slightly thickened at the upper area, though there is notable spatial variability. Despite the extensive supraglacial debris cover in the ablation zone, such that the insulation effect is widely expected, glacier surface lowering is remarkable except for the lowermost reach (Figs. 2a and 3a). The debris-covered section of the glacier extends from 4500 to 5850 m a.s.l., covering 14.9 km^2 (25% of the entire glacier), along which the area-

The Cryosphere Discuss., doi:10.5194/tc-2016-202, 2016
Manuscript under review for journal The Cryosphere
Published: 26 September 2016

weighted average of rate to elevation change is –0.55 m a^{-1}. Further, the debris-covered area shows a more negative trend (–0.51 m a^{-1}) than that of debris-free ice around 5100-5850 m a.s.l. (–0.30 m a^{-1}), where the two rates co-exist (Figs. 3a).

For the lower ablation area, the measured rate of elevation change at respective elevation bands is used to estimate the mass change of the entire glacier (Fig. 3a). In each case, geodetic mass balance is calculated using the two density scenarios (Sect. 2.7 and Table 2). The final mass change estimate is the average of the four combinations of two assumptions regarding the rate of elevation change in the upper accumulation area and two density assumptions, yielding the geodetic mass balance of Kanchenjunga Glacier to be –0.14 ± 0.12 m w.e. a^{-1} for the studied period of 1975–2010.

3.3 Glacier surface velocity

Figure 2b shows the spatial distribution of the surface velocity of Kanchenjunga Glacier derived from two ALOS PRISM ortho-images acquired in March and December 2010. Overall, surface velocities show a general pattern, almost stagnant in the lowermost areas, moderate in the ablation areas, and faster in the mid-glacier areas, varying from 0 to 72 m a^{-1}. On the other hand, the velocities remarkably vary from one tributary to another, possibly influenced by glacier thickness and surface slope.

3.4 Supraglacial ponds

For the study period between 1975 and 2010, supraglacial ponds of Kanchenjunga Glacier increased in number by more than fourfold, from 8 to 35, with a significant tenfold expansion in total area from 0.014 to 0.16 km^2, which resulted in an increase in average size from 1710 to 4580 m^2 (Fig. 5a). Most of ponds were formed in the mid-ablation area between 4700 and 5400 m a.s.l. or between 5 and 18 km from the terminus. Although the lifetime of a supraglacial pond is totally unknown but expected to be a few to several years, ponds in 1975 are not found in 2010 around their neighbouring locations, implying that those ponds in 1975 disappeared either by deformation due to glacier dynamics or by drainage through englacial channels (Sakai et al., 2000).

4 Discussion

4.1 Topographic variables and elevation change

In order to evaluate the effects of topographic and other variables on elevation change of Kanchenjunga Glacier, longitudinal profiles of related variables are summarized at 200-m intervals along centreline of the glacier (Fig. 6). The rate of elevation change is moderately negative at the glacier terminus (–0.13 ± 0.20 m a^{-1} at 0-2 km and –0.48 ± 0.36 m a^{-1} at 2-5 km), whereas it is largely negative in the mid ablation area (–0.83 ± 0.38 m a^{-1} at 5–20 km) over the period of 1975–2010 (Fig. 6a). This profile of the rate of elevation change is similar to those in the other debris-covered glaciers in the Khumbu and Langtang regions, for which the similar methodology was used (Bolch et al., 2011; Ragettli et al., 2016). Elevation change of the glacier surface is controlled by surface mass balance and glacier dynamics, which compensate each other under the steady state conditions (Cuffey and Paterson, 2010). Slope, flow speed, and longitudinal gradient of flow speed, which are related to emergence velocity, are therefore calculated (Figs. 6c-6e). Although the distribution of ice thickness is definitely important for the emergence velocity, it is unobtainable from the remote sensing data.

The Cryosphere Discuss., doi:10.5194/tc-2016-202, 2016
Manuscript under review for journal The Cryosphere
Published: 26 September 2016

In general, the mass balance of the debris-free glacier increases negatively at lower elevations. On the other hand, debris thickness increases down-glacier with considerable spatial variability (Kirkbride and Warren, 1999; Nakawo et al., 1999). The melt rate is high if the debris cover is thin because of the effect of low albedo, while it greatly decreases under thicker debris because of the insulating effect (Mattson et al., 1993). Consequently, the high melting rate on debris-covered glaciers is typically found in the mid-ablation areas characterized by a thin debris cover, while the melting rate substantially decreases at the lowermost terminus because of thicker debris and toward higher elevations because of cooler air temperatures. Both elevation and longitudinal profiles of the rate of elevation change follow this trend (Figs. 3a and 6a). Although the rates of elevation change along tributaries show different profiles (Fig. 6a), relationships with elevation look more straightforward, in which the rates of elevation change increase negatively in a similar trend from higher to lower elevations (Fig. 7a). Along the main tributary (T3) below 5400 m a.s.l. or down-glacier from 18 km, on the other hand, the rate of elevation change is constant and then increases toward zero below 4900 m a.s.l. or down-glacier from 5 km (Figs. 6a and 7a). Despite this large variability, the rate of elevation change and elevation show a significant correlation for all tributaries ($n = 197$, $r = 0.35$, $p < 0.001$).

Among variables such as slope, flow speed, and gradient of flow speed (Figs. 7b-7d), which are expected to relate to emergence velocity sustaining the glacier surface, only flow speed exhibits a statistically significant correlation with the rate of elevation change ($n = 195$, $r = 0.48$, $p < 0.001$). In the rigid definition, differences among ice fluxes at a given section of glacier, for which flow speed and ice thickness are required, generate the emergence velocity. In this regard, the gradient of flow speed is expected to be correlated with the rate of elevation change (less gradient, more negative lowering). However, large variability of the rate of elevation change at slow speed surfaces suggests that the surface mass balance, which should be affected by debris distribution, is more likely to result in the observed distribution of down-wasting of Kangchenjunga Glacier for the studied period of 1975–2010 (Figs. 7c).

4.2 Elevation changes on debris-covered and -free surfaces

Rates of elevation change, where two surfaces co-exist, show similar or even slightly stronger thinning on debris-covered surfaces than that on debris-free surfaces (Fig. 3a). Together with the substantial thinning in the mid-ablation area mentioned above, this suggests that debris-covered surface has also experienced thinning comparable to that of the exposed ice surface, which is consistent with the results of Kääb et al. (2012) and Nuimura et al. (2012). These findings support the proposition that the role of debris mantles in glacier mass balance and glacio-hydrological models needs to be reassessed or treated like debris-free glaciers (e.g., Kääb et al., 2012).

4.3 Supraglacial ponds on surface lowering

A significant negative correlation between the size of supraglacial ponds in 2010 and rate of elevation change is found, indicating that at sites where larger supraglacial pond exist, the glacier surface is more down-wasted than at sites where smaller pond exists ($n = 35$, $r = 0.45$, $p < 0.01$, Fig. 5b). In addition, many ponds exhibit greater lowering than the lower bound of the debris-covered surface (Fig. 5c). As illustrated box plots in Fig. 5c, the rate of elevation change for supraglacial ponds ($–1.25 \pm 0.34$ m a^{-1}) is significantly more negative than that of the debris-covered surfaces up to 20 km from the terminus ($–0.74 \pm 0.42$ m a^{-1}). Supraglacial ponds and ice cliffs, which often co-exist, are the principal spots of extensive heat

The Cryosphere Discuss., doi:10.5194/tc-2016-202, 2016
Manuscript under review for journal The Cryosphere
Published: 26 September 2016

absorption (Sakai et al., 2000, 2002; Röhl, 2008; Steiner et al., 2015; Miles et al., 2016). The distribution of significant lowering of supraglacial ponds, which probably did not persist at the same location for decades, suggests that these hot spots may have repeated a development and decay cycle over a few to several years by changing their location, thus resulting in surface lowering comparable to that of a debris-free glacier, though it should be noted that ice cliffs are not always accompanied by ponds.

The substantial lowering at the mid debris-covered surface that was observed in Kanchenjunga Glacier (Fig. 5c) could encourage the formation of additional ponds or expansion of existing ponds, which would further enhance the surface lowering by increase melting. In addition, it is also expected that the substantially lowered glacier surface would be gentler and thus the flow speed would decrease, which should promote further surface lowering by decreasing the emergence velocity. Ragettli et al. (2016) demonstrated that the pond density highly correlated with stagnant tongue area where no glacier velocity was observed. Although the different indices are used, the significant surface lowering of Kanchenjunga Glacier is found at the place where pond exists or slow velocity. Total number, surface area, and average size of supraglacial ponds have significantly increased recently in the mid-ablation area (Fig. 5a). Considering the high rate of surface lowering, negligible flow speed, gentle surface slope, and several existing supraglacial ponds of notable size, a large supraglacial lake is expected to be formed in the mid debris-covered area when calving of the glacier terminus begins (Röhl, 2008; Sakai et al., 2009; Sakai and Fujita, 2010).

4.4 Comparison with Khumbu Glacier

The geodetic mass balance of Kanchenjunga Glacier (-0.14 ± 0.12 m a^{-1}) is compared with Khumbu Glacier, one of the most investigated debris-covered glaciers in the Himalayas (Fig. 1), for which three previous studies have calculated geodetic mass balances in different periods: -0.27 ± 0.08 m w.e. a^{-1} (Bolch et al., 2011), -0.35 ± 0.20 m w.e. a^{-1} (Nuimura et al., 2012), and -0.51 ± 0.19 m w.e. a^{-1} (Gardelle et al., 2013; Fig. 8). Two possible causes of the different geodetic mass balances are discussed here: 1) area contributions of accumulation and debris-covered areas and 2) the density of supraglacial ponds.

Based on the geodetic ELA assumption (Sect. 2.7), Kanchenjunga Glacier has an accumulation area of 32.4 km^2 above the gELA of 5800-5850 m and thus a gAAR of 0.54, whereas Khumbu Glacier has an accumulation area of 8.4 km^2 (gAAR of 0.41), for which the gELA of Kanchenjunga Glacier is adopted for Khumbu Glacier because the elevation profile of the rate of elevation change of Khumbu Glacier is highly variable (Fig. 9a). On the other hand, the debris-covered area ratio is 0.25 (15 km^2) for Kanchenjunga Glacier and 0.40 (8.2 km^2) for Khumbu Glacier (Fig. 9b). Because the profiles of rate of elevation change are similar in both glaciers (Fig. 9a), greater accumulation areas and smaller debris-covered areas within the entire area of Kanchenjunga Glacier might contribute to the less negative geodetic mass balance compared with that of Khumbu Glacier (Fig. 9b).

As discussed above (Sect. 4.3), supraglacial ponds may play a key role in the down-wasting of the debris-covered area. Supraglacial ponds on Khumbu Glacier delineated from ALOS PRISM images (October 2008) are therefore compared with those on Kanchenjunga Glacier (Table 3). Major variables of supraglacial ponds, such as number, total area, pond area ratio to debris-covered area, and pond density, are roughly two to four times greater for Khumbu Glacier than Kanchenjunga Glacier, though the average pond area is similar (Table 3). This high pond density should have caused slightly negative rate of elevation change around 5100 m a.s.l. (Fig. 9a) and thus likely contributed to the more negative geodetic mass balance of

The Cryosphere Discuss., doi:10.5194/tc-2016-202, 2016
Manuscript under review for journal The Cryosphere
Published: 26 September 2016

Khumbu Glacier. The pond density, which has not been analyzed in wide regions and may be highly variable in time, could be an important factor for regionally contrasting geodetic mass balances along the Himalayas-Karakorum range (Kääb et al., 2012; Gardelle et al., 2013).

4.5 Representativeness of geodetic mass balance

Figure 8 also shows an area-weighted average of geodetic mass balance of five debris-covered glaciers in the Langtang region (–0.22 ± 0.13 m w.e. a^{-1}, Ragettli et al., 2016). Although it is similar to that of Khumbu Glacier, the individual mass balances are highly heterogeneous, which range between –0.10 and –0.43 m w.e. a^{-1}. On the other hand, the geodetic mass balances in the Khumbu region are similar each other except for one glacier contacting proglacial moraine-dammed lake, which strongly accelerates the thinning rate of the glacier (Bolch et al., 2011; Nuimura et al., 2012) whereas no proglacial lake exists in the five glaciers in Langtang (Ragettli et al., 2016). It should be noted that multiple glaciers have to be analyzed in a region if climatic impact on changing glaciers and its regional difference are discussed while a single glacier is intensively analyzed in this study.

5 Conclusions

This study provides the geodetic mass balance of Kanchenjunga Glacier, an extensively debris-covered glacier situated in the easternmost Nepal Himalaya, using two DEMs at high-resolution (5-m) spanning 35 years, Hexagon KH-9 (1975) and ALOS PRISM (2010) stereo-images. The rate of elevation change over the debris-covered surface is similar to that over the debris-free surface, even though it is widely expected that the insulating effect of debris suppresses the ice melting underneath. Considering the largely negative elevation change in the mid-ablation area, the debris-covered surface has also experienced thinning comparable to that of a debris-free glacier surface. The rate of elevation change shows a significant correlation with flow speed. Large variability of the rate of elevation change at slow speeds suggests that the surface mass balance, which may be affected by debris distribution, is more significant for the observed distribution of surface lowering of Kangchenjunga Glacier. Along the longitudinal profile of the rate of elevation change, many ponds show greater lowering than debris-covered area, meaning that the supraglacial ponds and associated ice cliffs may be a major constituent of intense ice wastage and play a significant role in heterogeneous surface lowering of debris-covered glaciers.

The elevation profile of the rate of elevation change is similar to that of Khumbu Glacier, one of the most intensively investigated glaciers in the Himalayas, but the area-weighted average mass balance of Kanchenjunga Glacier is less negative than those of Khumbu Glacier. This discrepancy should be attributed to greater accumulation areas and smaller debris-covered areas within the entire area of Kanchenjunga Glacier compared to those of Khumbu Glacier. Lower pond density may also play a key role in causing the less negative geodetic mass balance of Kanchenjunga Glacier.

This study demonstrates that DEMs generated with high-resolution satellite stereo-images can be used for examining the effect of supraglacial ponds on debris-covered glaciers, thus facilitating volumetric change analysis over time. The study highlights how a large debris-covered glacier, for which few studies have been done so far, has been dynamically changing over time and notes that the results of volumetric change analysis are different glacier to glacier, suggesting that a one-size-fits-all approach may not be applicable.

Author contribution. D. Lamsal and A. Sakai designed the study. D. Lamsal and K. Fujita analysed data and wrote the manuscript. All authors equally contributed to discussion of the study.

Acknowledgements. This study was supported by a grant from the Funding Program for Next Generation World-Leading Researchers (NEXT Program, GR052) and JSPS-KAKENHI grant Number 26257202.

References

Bolch, T., Pieczonka, T., and Benn, D. I.: Multi-decadal mass loss of glaciers in the Everest area (Nepal Himalaya) derived from stereo imagery, The Cryosphere, 5, 349–358, doi:10.5194/tc-5-349-2011, 2011.

Bolch, T., Kulkarni, A., Kääb, A., Huggel, C., Paul, F., Cogley, J. G., Frey, H., Kargel, J. S., Fujita, K., Scheel, M., Bajracharya, S., and Stoffel, M.: The state and fate of Himalayan glaciers, Science, 336, 310–314, doi:10.1126/science.1215828, 2012.

Cuffey, K. and Paterson, W. S. B.: The Physics of Glaciers, Elsevier, Butterworth-Heineman, Burlington, MA, USA, 2010.

Fujita, K. and Nuimura, T.; Spatially heterogeneous wastage of Himalayan glaciers, P. Natl. Acad. Sci. USA, 108, 14011–14014, doi:10.1073/pnas.1106242108, 2011.

Fujita, K., Sakai, A., Nuimura, T., Yamaguchi, S., and Sharma, R. R.: Recent changes in Imja Glacial Lake and its damming moraine in the Nepal Himalaya revealed by in situ surveys and multi-temporal ASTER imagery, Environ. Res. Lett., 4, 045205, doi:10.1088/1748-9326/4/4/045205, 2009.

Gardelle, J., Berthier, E., Arnaud, Y., and Kääb, A.: Region-wide glacier mass balances over the Pamir-Karakoram-Himalaya during 1999–2011, The Cryosphere, 7, 1263–1286, doi:10.5194/tc-7-1263-2013, 2013.

Han, H., Wang, J., Wei, J., and Liu, S.: Backwasting rate on debris-covered Koxkar glacier, Tuomuer mountain, China, J. Glaciol., 56, 287–296, doi:10.3189/002214310791968430, 2010.

Heid, T., and Kääb, A.: Repeat optical satellite images reveal widespread and long term decrease in land-terminating glacier speeds, The Cryosphere, 6, 467–478, doi:10.5194/tc-6-467-2012, 2012.

Kääb, A., Berthier, E., Nuth, C., Gardelle, J., and Arnaud, Y.: Contrasting patterns of early twenty-first-century glacier mass change in the Himalayas, Nature, 488, 495–498, doi:10.1038/nature11324, 2012.

Kirkbride, M. P., and Warren, C. R.: Tasman Glacier, New Zealand: 20th-century thinning and predicted calving retreat, Global Planet. Change, 22, 11–28, 1999.

Lamsal, D., Sawagaki, T., and Watanabe, T.: Digital terrain modelling using Corona and ALOS PRISM data to investigate the distal part of Imja Glacier, Khumbu Himal, Nepal, J. Mt. Sci., 8, 390–402, doi:10.1007/s11629-011-2064-0, 2011.

Leprince, S., Barbot, S., Ayoub, F., and Avouac, J. P.: Automatic and precise orthorectification, co-registration, and subpixel correlation of satellite images, application to ground deformation measurements, IEEE Trans. Geosci. Remote Sens., 45, 1529–1558, doi:10.1109/TGRS.2006.888937, 2007.

Mattson, L. E., Gardner, J. S., and Young, G. J.: Ablation on debris covered glaciers: an example from the Rakhiot Glacier, Punjab, Himalaya, IAHS Publication, 218, 289–296, 1993.

Miles, E. S., Pellicciotti, F., Willis, I. C., Steiner, J. F., Buri P., and Arnold, N. S.: Refined energy-balance modelling of a supraglacial pond, Langtang Khola, Nepal, Ann. Glaciol., 57(71), 29–40, doi:10.3189/2016AoG71A421, 2016.

Nakawo, M., Yabuki, H., and Sakai, A.: Characteristics of Khumbu Glacier, Nepal Himalaya: recent changes in the debris-covered area, Ann. Glaciol., 28, 118–122, 1999.

Nuimura, T., Fujita, K., Fukui, K., Asahi, K., Aryal, R., and Ageta, Y.: Temporal changes in elevation of the debris-covered ablation area of Khumbu glacier in the Nepal Himalaya since 1978, Arct. Antarct. Alp. Res., 43, 246–255, doi:10.1657/1938-4246-43.2.246, 2011.

Nuimura, T., Fujita, K., Yamaguchi, S., and Sharma, R. R.: Elevation changes of glaciers revealed by multitemporal digital elevation models calibrated by GPS survey in the Khumbu region, Nepal Himalaya, 1992–2008, J. Glaciol., 58, 648–656, doi:10.3189/2012JoG11J061, 2012.

Ojha, S., Fujita, K., Asahi, K., Sakai, A., Lamsal, D., Nuimura, T., and Nagai, H.: Glacier area shrinkage in eastern Nepal Himalaya since 1992 using high-resolution inventories from aerial photographs and ALOS satellite images. J. Glaciol., 62, 512-524, doi:10.1017/jog.2016.61, 2016

Pellicciotti, F., Stephan, C., Miles, E., Herreid, S., Immerzeel, W. W., and Bolch, T.: Mass-balance changes of the debris-covered glaciers in the Langtang Himal, Nepal, from 1974 to 1999, J. Glaciol., 61, 373–386, doi:10.3189/2015JoG13J237, 2015.

Pieczonka, T., Bolch, T., Wei, J., and Liu, S.: Heterogeneous mass loss of glaciers in the Aksu-Tarim Catchment (Central Tien Shan) revealed by 1976 KH-9 Hexagon and 2009 SPOT-5 stereo imagery, Remote Sens. Environ., 130, 233–244, doi:10.1016/j.rse.2012.11.020, 2013.

Racoviteanu, A. E., Arnaud, Y., Williams M. W., and Manley, W. F.: Spatial patterns in glacier characteristics and area changes from 1962 to 2006 in the Kanchenjunga–Sikkim area, eastern Himalaya, The Cryosphere, 9, 505–523, doi: 10.5194/tc-9-505-2015, 2015.

Ragettli, S., Bolch, T., and Pellicciotti, F.: Heterogeneous glacier thinning patterns over the last 40 years in Langtang Himal, Nepal, The Cryosphere, 10, 2075-2097, doi:10.5194/tc-10-2075-2016, 2016.

Röhl, K.: Characteristics and evolution of supraglacial ponds on debris-covered Tasman Glacier, New Zealand, J. Glaciol., 54, 867–880, doi:10.3189/002214308787779986, 2008.

Sakai, A., and Fujita, K.: Formation conditions of supraglacial lakes on debris-covered glaciers in the Himalayas, J. Glaciol., 56, 177–181, doi:10.3189/002214310791190785, 2010.

Sakai, A., Nakawo, M., and Fujita, K.: Melt rate of ice cliffs on the Lirung Glacier, Nepal Himalayas, 1996, Bull. Glacier Res., 16, 57–66, 1998.

Sakai, A., Takeuchi, N., Fujita, K., and Nakawo, M.: Role of supraglacial ponds in the ablation processes of a debris-covered glacier in the Nepal Himalayas, IAHS Publication, 264, 119–130, 2000.

Sakai, A., Nakawo, M., and Fujita, K.: Distribution characteristics and energy balance of Ice cliffs on debris-covered glaciers, Nepal Himalaya, Arct. Antarct. Alp. Res., 34, 12–19, 2002.

Sakai, A., Nishimura, K., Kadota, T., and Takeuchi, N.: Onset of calving at supraglacial lakes on debris covered glaciers of the Nepal Himalayas, J. Glaciol., 55, 909–917, doi:10.3189/002214309790152555, 2009.

Salerno, F., Guyennon, N., Thakuri, S., Viviano, G., Romano, E., Vuillermoz, E., Cristofanelli, P., Stocchi, P., Agrillo, G., Ma, Y., and Tartari, G.: Weak precipitation, warm winters and springs impact glaciers of south slopes of Mt. Everest (central Himalaya) in the last 2 decades (1994–2013), The Cryosphere, 9, 1229–1247, doi:10.5194/tc-9-1229-2015, 2015.

The Cryosphere Discuss., doi:10.5194/tc-2016-202, 2016
Manuscript under review for journal The Cryosphere
Published: 26 September 2016

Scherler, D., Leprince, S., and Strecker M. R.: Glacier-surface velocities in alpine terrain from optical satellite imagery–Accuracy improvement and quality assessment, Remote Sens. Environ., 112, 3806–3819, 2008.

Steiner, J. F., Pellicciotti, F., Buri, P., Miles, E. S., Immerzeel W. W., and Reid, T. D.: Modeling ice-cliff backwasting on a debris-covered glacier in the Nepalese Himalaya, J. Glaciol., 61, 889–907, doi:10.3189/2015JoG14J194, 2015.

Surazakov, A. B., and Aizen, V. B.: Positional accuracy evaluation of declassified Hexagon KH-9 mapping camera imagery, Photogramm. Eng. Remote Sens., 76, 603–608, 2010.

Tachikawa T., Hato, M., Kaku, M., and Iwasaki, A.: The characteristics of ASTER GDEM version 2, Proc. IGARSS 2011 Symposium, Vancouver, Canada, 24–29 July 2011, 3657–3660, 2011.

Zhang, Y., Fujita, K., Liu, S., Liu, Q., and Nuimura, T.: Distribution of debris thickness and its effect on ice melt at Hailuogou Glacier, southeastern Tibetan Plateau, using in situ surveys and ASTER imagery, J. Glaciol., 57, 1147–1157, doi:10.3189/002214311798843331, 2011.

The Cryosphere Discuss., doi:10.5194/tc-2016-202, 2016
Manuscript under review for journal The Cryosphere
Published: 26 September 2016

Table 1. Remote sensing data used in this study for generating digital elevation models (DEMs), mapping debris-covered and debris-free glacier surfaces and supraglacial ponds, and computing surface velocity and elevation data for orthorectification of satellite imageries.

Sensor/Sensor mode	Acquisition date	Resolution (m)	ID
Hexagon/Stereo	20 December 1975	7.6	DZB1211-500057L036001 DZB1211-500057L037001 DZB1211-500057L038001
ALOS PRISM/Stereo	9 March 2010	2.5	ALPSMF219552985 ALPSMN219553040 ALPSMB219553095
ALOS PRISM/Stereo	10 December 2010	2.5	ALPSMF259812985 ALPSMN259813040 ALPSMB259813095
ALOS PRISM/Nadir	24 October 2008	2.5	ALPSMN045823035 ALPSMN045823040
ASTER GDEM2	Composite since 2000	30.0	ASTGTM2_N27E087 ASTGTM2_N27E088 ASTGTM2_N28E087 ASTGTM2_N28E088

The Cryosphere Discuss., doi:10.5194/tc-2016-202, 2016
Manuscript under review for journal The Cryosphere
Published: 26 September 2016

Table 2. Area-weighted geodetic mass balance of Kangchenjunga Glacier for the period 1975-2010 (m w.e. a^{-1}). Two cases for the rate of elevation change where continuous digital elevation models are unavailable, and two density scenarios are also assumed (see Sect. 2.5 and 2.6).

dh/dt of unmeasured area	Case 1: +0.01 m a^{-1}		Case 2: +0.11 m a^{-1}	
Density assumption	Scenario 1	Scenario 2	Scenario 1	Scenario 2
Mass balance	–0.149	–0.151	–0.121	–0.137
Averaged mass balance	–0.14 ± 0.12			

The Cryosphere Discuss., doi:10.5194/tc-2016-202, 2016
Manuscript under review for journal The Cryosphere
Published: 26 September 2016

Table 3. Attributes of supraglacial ponds (≥ 1000 m^2) in the debris-covered area of Kanchenjunga (December 2010) and Khumbu (October 2008) glaciers.

Glacier	n	A_p (km^2)	a_p (m^2)	A_d (km^2)	R_p (%)	D_p (km^{-1})
Kanchenjunga	35	0.160	4580	15.0	1.1	2.3
Khumbu	74	0.302	4090	8.2	3.7	9.0

n: number of ponds, A_p: total area of ponds, a_p: average area of pond, A_d: debris-covered area, R_p: ratio of pond to debris-covered areas, and D_p: pond density.

5

The Cryosphere Discuss., doi:10.5194/tc-2016-202, 2016
Manuscript under review for journal The Cryosphere
Published: 26 September 2016

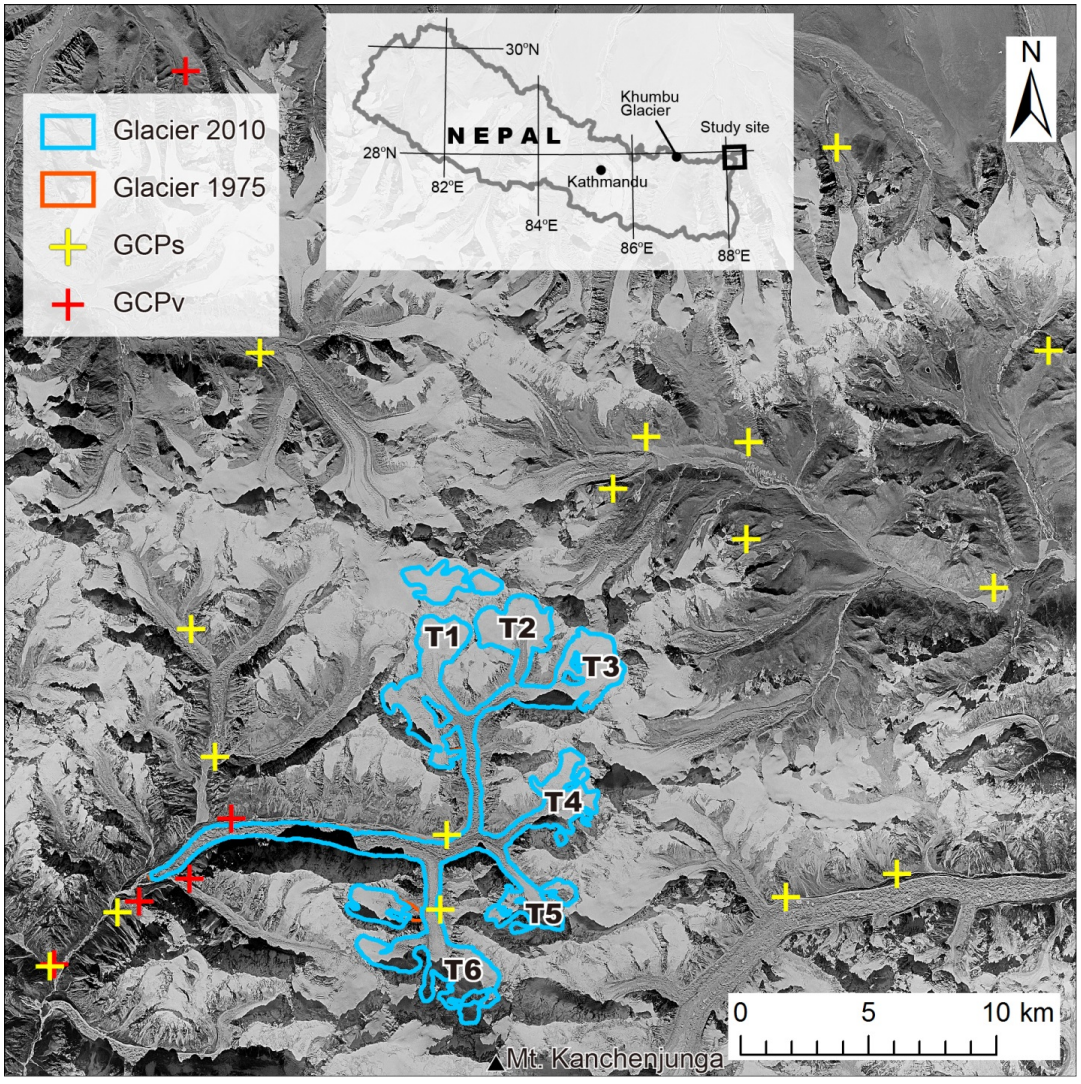

Figure 1. Outline of Kanchenjunga Glacier with 21 ground control points (GCPs) shown on a Hexagon KH-9 image taken in 1975. Five of the 21 GCPs are used to validate the accuracy of transformation (GCPv). Major tributaries are defined as T1 to T6.

The Cryosphere Discuss., doi:10.5194/tc-2016-202, 2016
Manuscript under review for journal The Cryosphere
Published: 26 September 2016

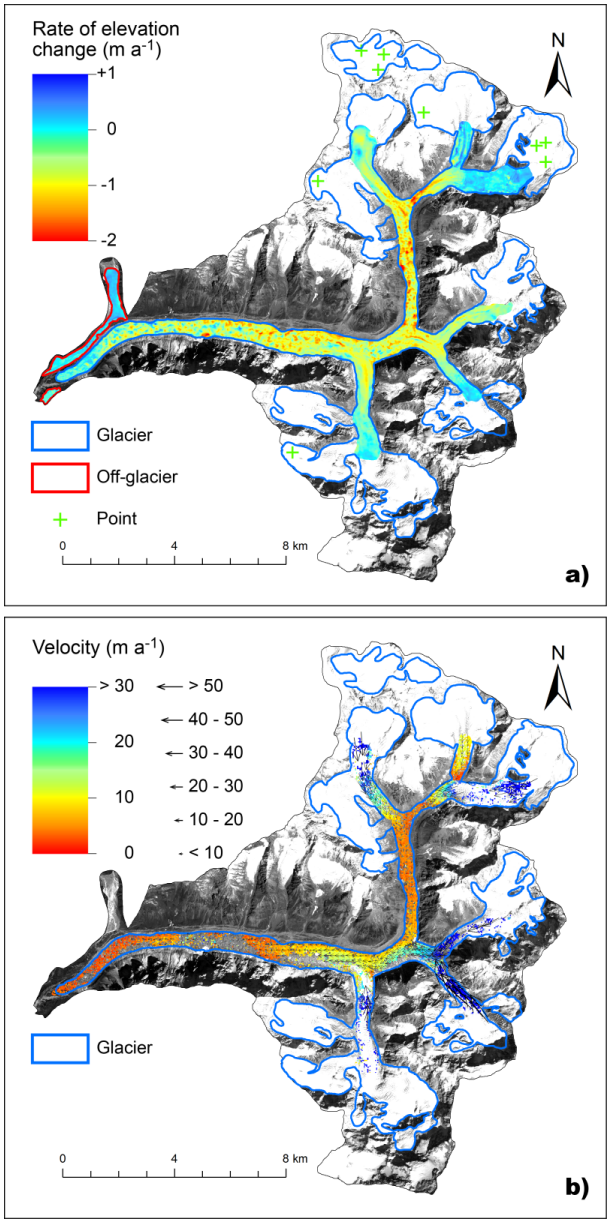

Figure 2. Spatial distributions of (a) the rate of elevation change for the period of 1975–2010 and (b) surface velocity between March and December of 2010 for Kanchenjunga Glacier. The elevation difference in the off-glacier area (outlined by the red polygon) is used to evaluate the relative uncertainty of two digital elevation models (DEMs). The green crosses in (a) denote point measurements of elevation change in the upper accumulation area where poorly contrasted surfaces hamper DEM creation. Vectors in (b) are depicted at a 200-m spatial interval for better visibility.

The Cryosphere Discuss., doi:10.5194/tc-2016-202, 2016
Manuscript under review for journal The Cryosphere
Published: 26 September 2016

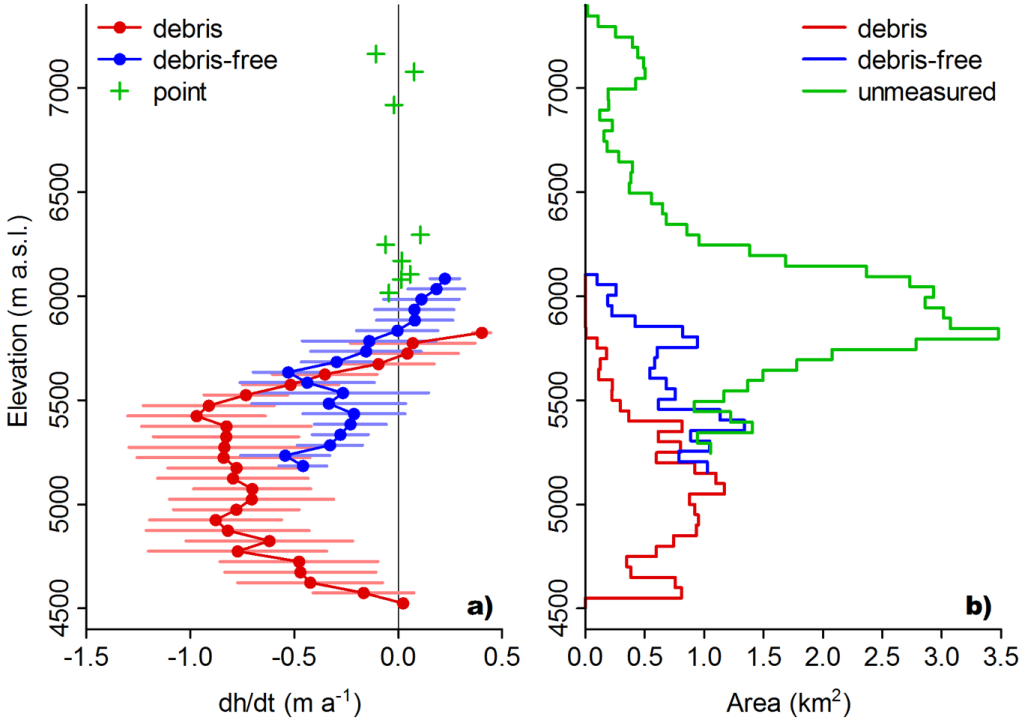

Figure 3. Elevation profiles of (a) the rate of elevation change (dh/dt) and (b) hypsometry of Kangchenjunga Glacier at 50-m elevation bands. Red and blue denote debris-covered and debris-free surfaces, respectively. Bars represent standard deviations within the respective band. The green crosses and green line denote point measurements in the upper accumulation area (Fig. 2a) and the area distribution of the unmeasured part, respectively.

The Cryosphere Discuss., doi:10.5194/tc-2016-202, 2016
Manuscript under review for journal The Cryosphere
Published: 26 September 2016

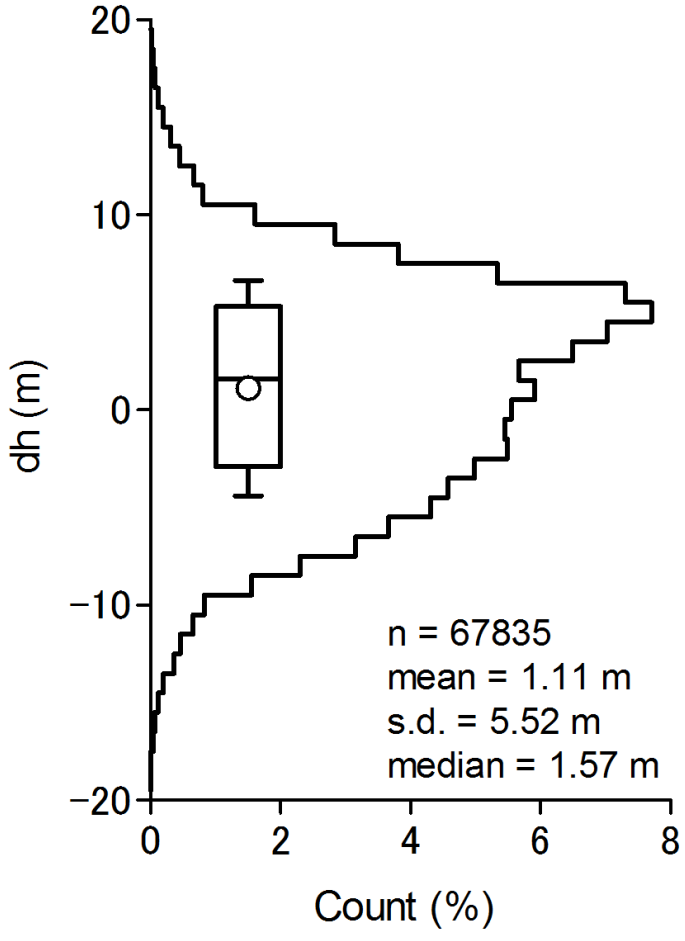

Figure 4. Histogram (1-m bin) and box plot of elevation difference (dh) between two digital elevation models in the off-glacier area (Fig. 2a). Box, thick line, circle, and whiskers denote interquartile, median, mean, and standard deviations, respectively.

The Cryosphere Discuss., doi:10.5194/tc-2016-202, 2016
Manuscript under review for journal The Cryosphere
Published: 26 September 2016

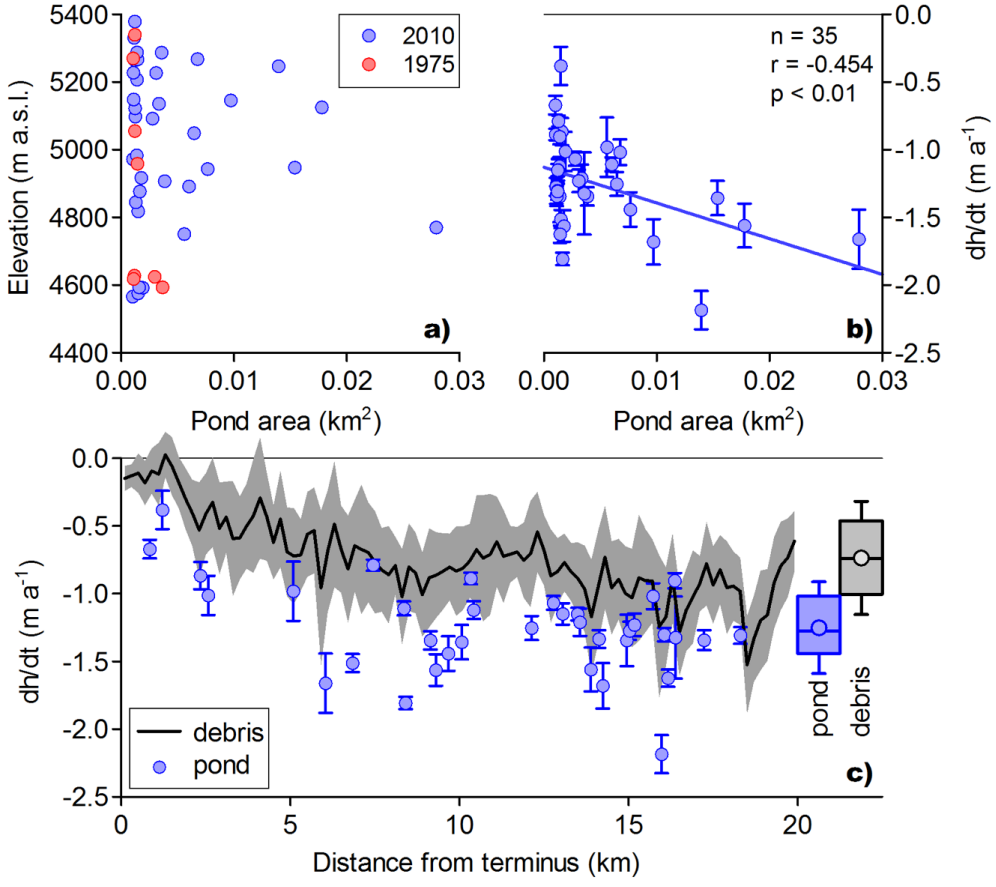

Figure 5. Supraglacial ponds (> 1000 m2) in the debris-covered area of Kanchenjunga Glacier. (a) Elevation distributions of ponds in 1975 and 2010. (b) Relationship between pond area and rate of elevation change (dh/dt). (c) Longitudinal profile and box plot of rate of elevation change (dh/dt) of the debris-covered area and ponds. Box, thick line, circle, and whiskers denote interquartile, median, mean, and standard deviations, respectively.

The Cryosphere Discuss., doi:10.5194/tc-2016-202, 2016
Manuscript under review for journal The Cryosphere
Published: 26 September 2016

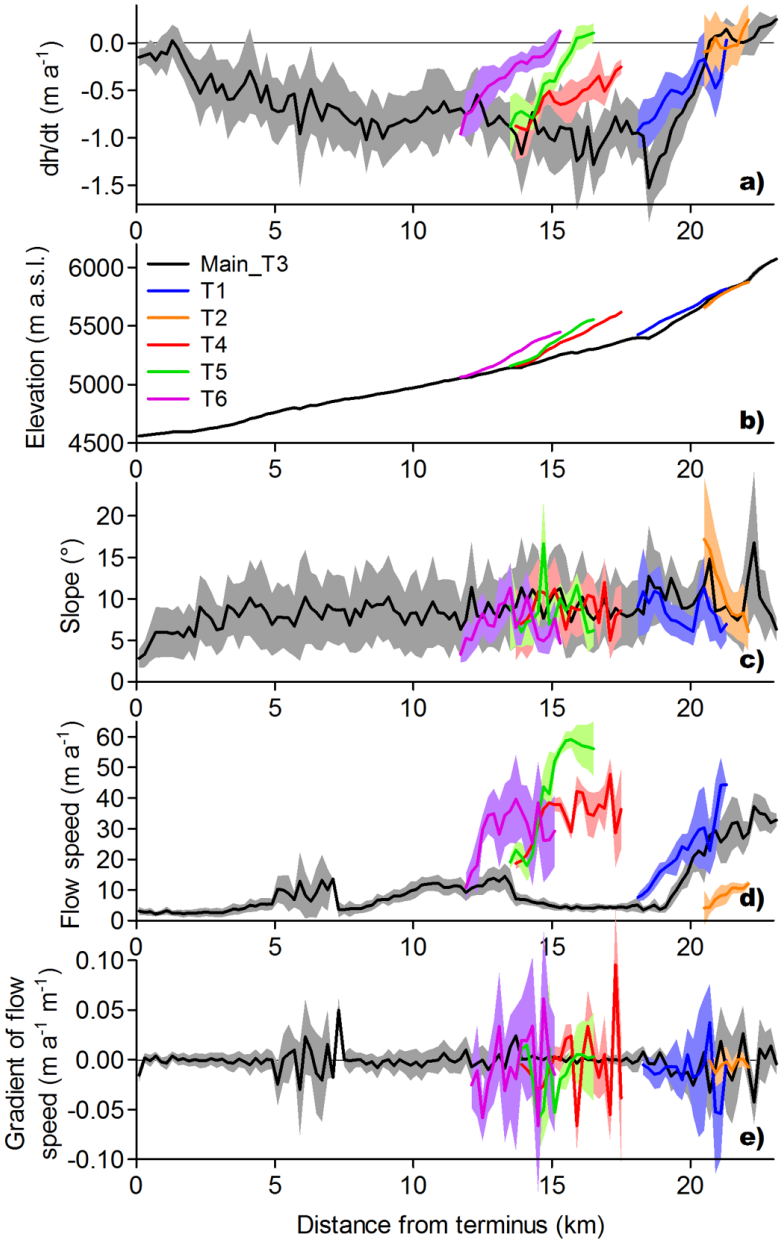

Figure 6. Longitudinal profiles of (a) the rate of elevation change (dh/dt), (b) elevation, (c) slope, (d) flow speed, and (e) gradient of flow speed of Kanchenjunga Glacier. Tributaries are defined in Fig. 1. All parameters are calculated at 200-m intervals along the centreline, which is manually drawn.

The Cryosphere Discuss., doi:10.5194/tc-2016-202, 2016
Manuscript under review for journal The Cryosphere
Published: 26 September 2016

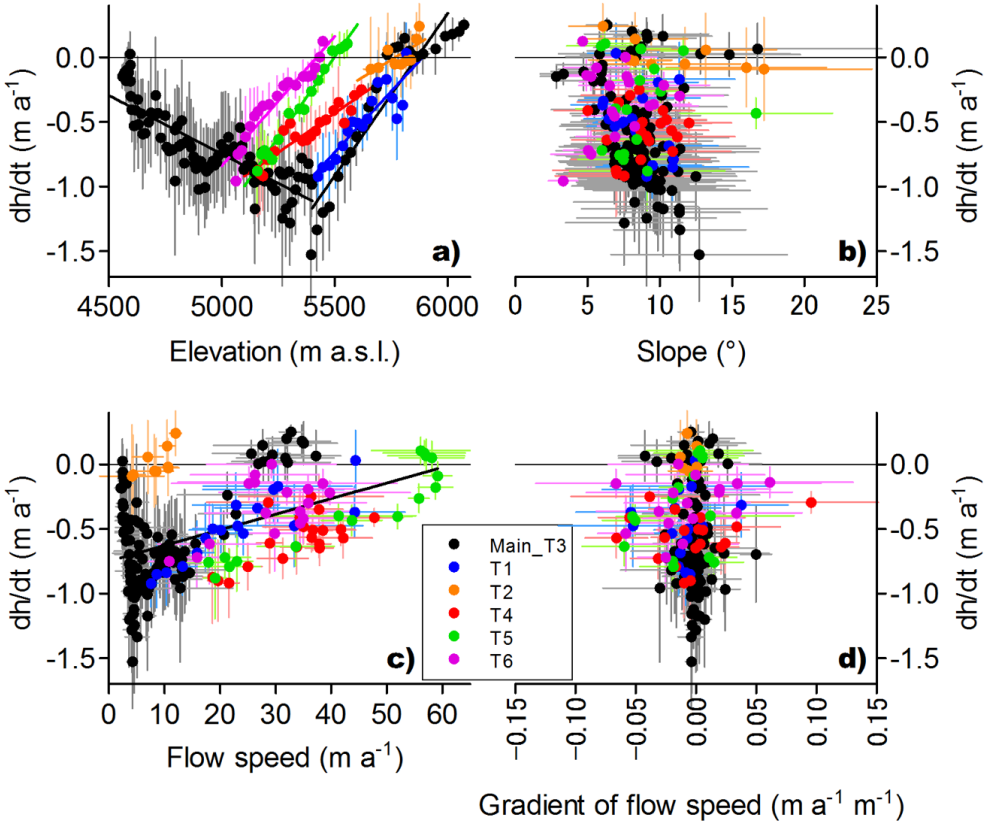

Figure 7. Scatterplots of (a) elevation, (b) slope, (c) flow speed, and (d) gradient of flow speed with respect to the rate of elevation change (dh/dt) for Kanchenjunga Glacier. Tributaries are defined in Fig. 1. Linear regressions in (a) are obtained for each tributary, while that in (c) is obtained for all tributaries. The main tributary T3 is divided at 5400 m a.s.l. for the regression calculations (black lines in a).

The Cryosphere Discuss., doi:10.5194/tc-2016-202, 2016
Manuscript under review for journal The Cryosphere
Published: 26 September 2016

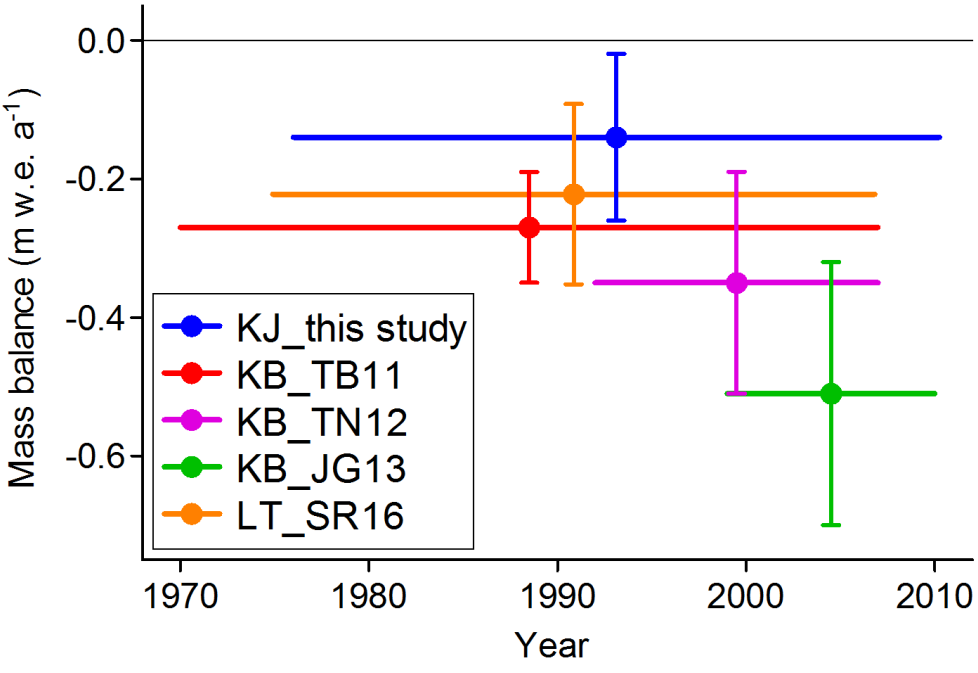

Figure 8. Geodetic mass balance of Kanchenjunga Glacier (KJ: 1975-2010, this study) compared with those of Khumbu Glacier (KB) from three previous studies (TB11: 1970-2007, Bolch et al., 2011; TN12: 1992-2008, Nuimura et al., 2012; JG13: 1999-2011, Gardelle et al., 2013). Also shown is area-weighted geodetic mass balance of five debris-covered glaciers in Langtang (SR16: 1975-2006, Ragettli et al., 2016). Note that the error range of SR16 is standard deviation of geodetic mass balance of five glaciers while the others are of each study.

The Cryosphere Discuss., doi:10.5194/tc-2016-202, 2016
Manuscript under review for journal The Cryosphere
Published: 26 September 2016

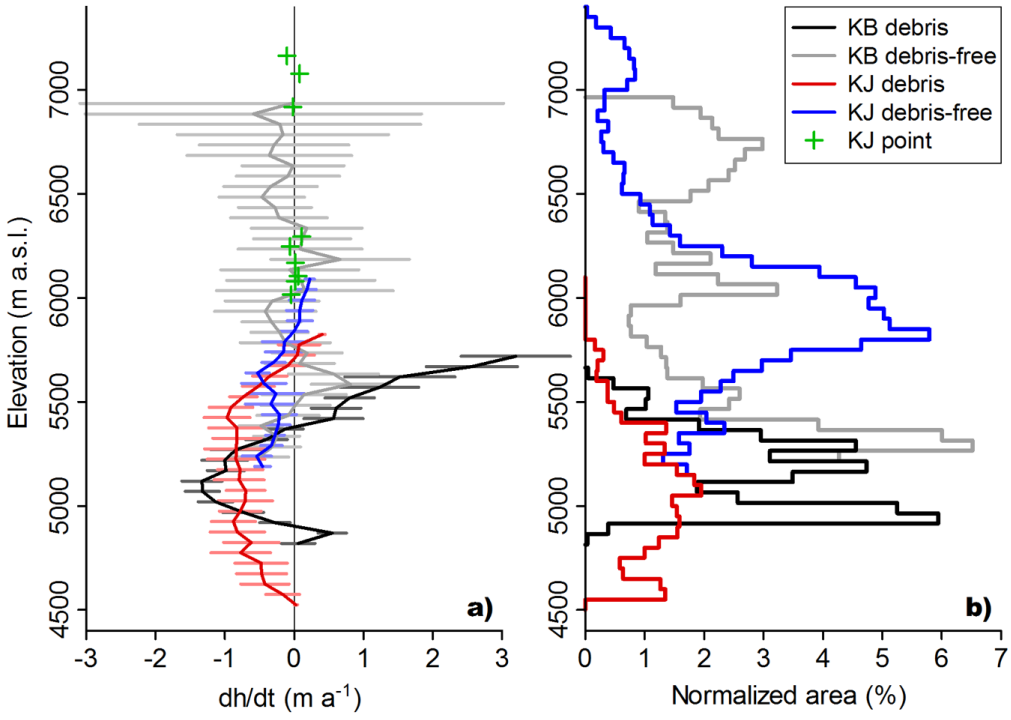

Figure 9. Elevation profiles of (a) the rate of elevation change (dh/dt) and (b) normalized hypsometry of Kangchenjunga (KJ) and Khumbu (KB) Glaciers at 50-m elevation bands. The data for Khumbu Glacier is from Nuimura et al. (2012). Red and black lines denote debris-covered, and blue and gray lines denote debris-free surfaces. Bars represent the standard deviation within a respective band. Green crosses denote point measurements in the upper accumulation area (Fig. 2a).